Semi-Automated Glioblastoma Tumor Detection Based on Different Classifiers Using Magnetic Resonance Spectroscopy

Ayob Faramarzi [1], Nazila Loghmani [2], Roqaie Moqadam [3,4], Armin Allahverdy [5], Meysam Siyah Mansoory [1,*] ID

[1] Department of Biomedical Engineering, School of Medicine, Kermanshah University of Medical Sciences, Kermanshah, Iran

[2] Biomedical Engineering Department, Faculty of Engineering, University of Isfahan, Isfahan, Iran

[3] Neuroimaging and Analysis Group, Research Center for Molecular and Cellular Imaging, Advanced Medical Technologies and Equipment Institute, Tehran University of Medical Sciences, Tehran, Iran

[4] Department of Medical Physics & Biomedical Engineering, School of Medicine, Tehran University of Medical Sciences, Tehran, Iran

[5] Department of Radiology, Sari School of Allied Medical Sciences, Mazandaran University of Medical Sciences, Sari, Iran

*Corresponding Author: Meysam Siyah Mansoory
  Email: meysam.smansoory@kums.ac.ir

Abstract

Purpose: Glioblastoma Multiform (GBM) is one of the most common and deadly malignant brain tumors. Surgery is the primary treatment, and careful surgery can minimize recurrence odds. Magnetic Resonance Imaging (MRI) imaging with Magnetic Resonance Spectroscopy (MRS) is used to diagnose various types of tumors in the Central Nervous System (CNS). In this study, several classification methods were used to separate tumor and healthy tissue.

Materials and Methods: This study examined the MRI and MRS results of seven people enrolled in this study in 2018. The data was obtained with a prescription from a neurologist and neurosurgeon. Choline (Cho) and N-Acetylaspartate (NAA) metabolite signals were selected as the reference signal after preprocessing and removing the water signal. With the support of 3 radiologists, each tumor and healthy vesicles were identified for every patient. Then, tumor and healthy voxels were separated based on Multilayer Perceptron (MLP), linear Support Vector Machine (SVM), Gaussian SVM, and Fuzzy system using the obtained values and four different methods.

Results: Data extracted from Cho and NAA metabolites were fed into MLP, linear SVM, Gaussian and Fuzzy SVM as input, and the amounts of accuracy, sensitivity, and specificity were determined for each method. The maximum accuracy for training mode and test mode was equal to 89.7% and 87%, respectively, specific to classification using Gaussian SVM. The results also showed that the classification accuracy can be significantly increased by increasing the number of fuzzy membership functions from 2 to 6.

Conclusion: The results of this study suggested that a more complex classification system, such as SVM with a Gaussian kernel and fuzzy system can be more efficient and reliable when it comes to separating tumor tissue from healthy tissues from MRS data.

Keywords: Magnetic Resonance Spectroscopy; Support Vector Machine; Fuzzy; Multi-Layer Perceptron.

1. Introduction

The World Health Organization (WHO) refers to a fourth-degree brain glioma as a glioblastoma, which is a type of brain cancer that accounts for approximately 75% of high-grade brain tumors [1]. This form of glioma is called GBM because it can take several different morphological forms. GBM is the most common and deadly primary malignant brain tumor, with an incidence of 3.2 cases per 100,000 population per year [2, 3]. The average lifespan of patients with this deadly tumor is 15-18 months [4]. To date, glioblastoma remains incurable despite advances in imaging, chemotherapy, and radiation therapy. The initial treatment for GBM is surgery, and the more accurate the surgical procedure, the better chance of survival and the lower the chance of tumor recurrence [5, 6]. Because GBM tissue is very similar to brain tissue [7], imaging techniques can assess the tumor more effectively between healthy and tumor waxes. Emerging non-invasive imaging techniques provide information on tissue properties, structure, and metabolic processes [8].

MRI shows morphological and anatomical features of the disease. Therefore, MRI is frequently used in the diagnosis and follow-up treatment of glioblastoma tumors [9]. MRS is also a non-invasive method that allows the identification and measurement of tissue metabolites. In some cases, a combination of conventional MRI and MRS is often used to diagnose and monitor various diseases, including neurological disorders, especially in the CNS, such as stroke, brain tumors, and mental disorders [10].

Anatomical imaging does not differentiate between tumor progression, radiation necrosis, and edema; therefore, conventional MRI images cannot be used for this purpose [11]. Because there are differences in a tumor's metabolic structure, radiation necrosis, and edema, MRS imaging is used to diagnose these areas [11].

Different metabolites are found in different tissues, and the levels of these metabolites can fluctuate based on diseases. Essentially, metabolic changes are indicators of disease onset and improvement. This is mainly because metabolic changes become evident earlier than anatomical changes. Furthermore, as previously mentioned, brain tissue's biochemical profile can be measured by (MRI) using MRS [12]. MRS data is received as frequency spectra from the device. The received FID signal must be analyzed to determine the concentration of each metabolite.

FID analysis is done with different software. TARQUIN is one of the most commonly used software for this purpose. TARQUIN uses a base set to calculate the concentration of metabolites, and the base set used in TARQUIN is obtained from the simulation of quantum mechanics using predetermined parameters [13-17]. The concentration of each metabolite is calculated in the frequency spectrum with the level below the corresponding peak diagram [18]. MRS performs both single-voxel and multi-voxel spectroscopy. In the latter method, an arbitrary number of voxels is used for networking the specified range. Every networked part has its own spectrum. After the spectral analysis, the concentration of metabolites in each voxel is calculated. Some concentrations and ratios of metabolites can help determine whether voxels are healthy or tumorous. Artificial Intelligence (AI) and machine learning are currently being used to diagnose and predict disease [19]. Previous studies have suggested several techniques for differentiating brain tumors. However, in this study, four neural networks were used for the first time in the automatic diagnosis of tumors and healthy areas in glioblastoma based on MRS data. So the aim of this study is to make reliable discrimination between normal and tumor tissue, which normal tissue may contain edema.

Because there may be errors during a visual examination, especially if a tumor appears at the border, in this study, several automatic methods that differentiate tumor from non-tumor areas through neural networks were proposed to compare their results. Then, the strengths and weaknesses of each method are examined to determine most effective one.

2. Materials and Methods

2.1. Data Acquisition

The statistical population includes seven individuals (four males and three females) with a mean age of 47 ± 25 who had been diagnosed with multiform glioblastoma tumor (inclusion criteria). These patients were referred to Imam Khomeini Hospital in Tehran for MRI imaging and MRS analysis by a neurologist and a neurosurgeon in 2017. In this study multi-voxels data has been used, in other words, the learning vector contains voxels of tumor and normal tissue. The overall number of learning vector is 293, which contains voxels of tumor and normal tissue. Prior to performing the test (obtaining data), the research

process was fully explained to all patients, and they signed the consent form after they approved it.

In this study, the Siemens MAGNETOM Trio Tim 3T scanner was used. A large number of spectra (MRS data) are necessary to determine the extent of the tumor; therefore, all data were acquired using Chemical Shift Imaging (CSI). The CSI method also allows for the examination of focal and close points. This is extremely important for differentiating between tumor and non-tumor areas [20]. The parameters used in this study were MRI images with TE=83ms, TR=6000ms, ST=5/5ms, Inversion Time=2500 ms, Flip Angle=120, samples per pixel=1, Pixel Bandwidth=119 and measurement parameters for MRS data are TE=135ms and TR=1570ms, respectively. Imaging was performed using the PRESS method. The signal-to-noise ratio is shorter at short TE than at high TE; however, these data were collected using long TE because the spectrum shows more metabolites at short TE than at long TE, which causes more errors in the calculation. In addition, in long TE, water and fat signals have less destructive effects on the spectrum obtained. At higher TEs, the spectrum of metabolites is more distinct, and images obtained after contrast injection were used to select the VOI site for MRSI.

All tumor and healthy vascular cells were identified for each patient by three radiologists of Imam Reza Hospital, with the assistant professor's scientific rank from Kermanshah University of Medical Sciences. The standard was the maximum opinion of radiologists. The criteria for the determination of tumor and normal tissue voxels by radiologists were conventional MRI.

2.2. Preprocessing

First, the number of voxels in each dataset was determined by using Sivic software. Figure 1 shows that each MRI image has a specific region where a network of voxels is placed. Figure 1 shows that the region of studding tissue is limited to the normal and tumor voxels, which reduces the effect of diversity in brain metabolite.

The data was loaded into Tarquin at this point. The water signal is much larger than that of other metabolites; therefore, despite the presence of water in the FID, the software cannot accurately detect the other metabolites (Figure 2). Hence, water suppression should be performed first using Tarquin.

According to the convention, the horizontal axis is numbered from right to left [21]. Likewise, the fat effects
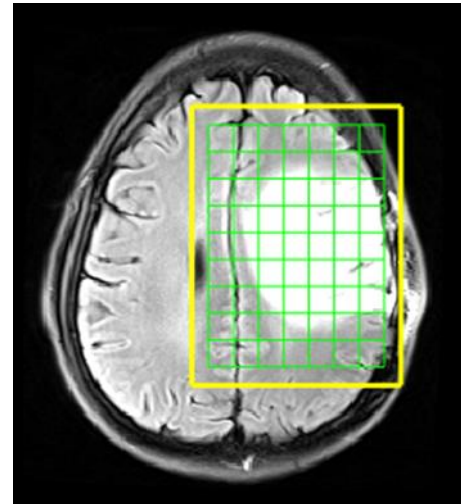

Figure 1. The yellow box indicates the region to be photographed, and the green grid indicates the number of voxels as well as the exact location of each voxel. While paying attention to the specific locations of each voxel, the radiologist comments on the tumor or the health of that voxel
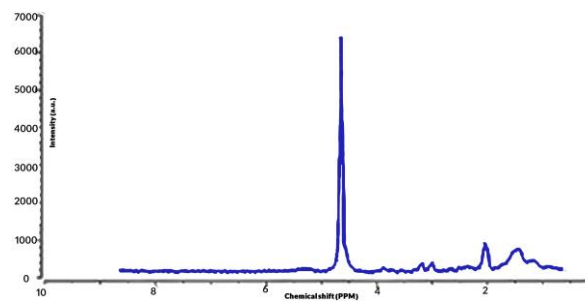

Figure 2. The FID signal is taken from the time domain to the frequency domain using Fourier transform. The signal is located at a 4.65 ppm water signal

should be removed from the FID. In Tarquin, water suppression is accomplished by HSVD [22]. The effect of this signal was removed to allow for further analysis of metabolite concentrations. When the water is suppressed as well as the fat is removed, the signal of other metabolites becomes available for analysis (Figure 3).
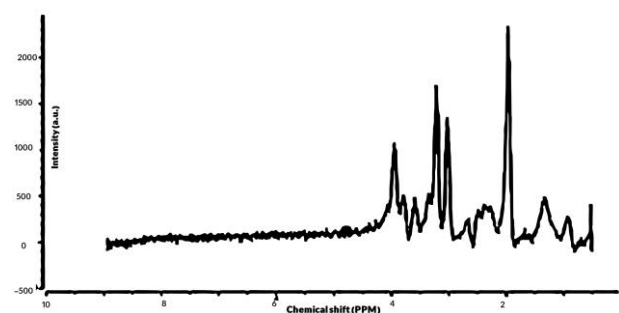

Figure 3. Here, the signals of the metabolites are more clearly visible than before the water suppression operation. NAA metabolites at 2.01 and Cho at 3.02

At this stage, Cho and NAA metabolites were chosen as reference signals (Figure 4). The concentration of each metabolite is obtained by choosing a reference for that metabolite. The concentration of each metabolite is proportional to its FID range (Figure 5).

After calculating NAA and Cho's concentration, the values were considered as the input for neural networks.

In this study, four methods were used to determine healthy tumor voxel: MLP, linear SVM, nonlinear SVM, and Fuzzy. Additionally, Perceptron is also a machine learning algorithm that falls under the category of supervised learning. The Perceptron algorithm works as a linear binary classification algorithm, meaning its predictions are calculated by looking at the weighted linear combination of the inputs [23].

Support vector machine is a supervised machine learning algorithm widely used in classifying problems. The backup vector machine algorithm identifies each data sample as a point in the n-dimensional space based on each property's value, one of the components of a point coordinate on the graph [24]. The fuzzy inference system transforms a knowledge base by means of a systematic process into a nonlinear mapping, thus making it useful in engineering applications, especially in decision-making [25].

2.3. Classification Methods

For classifying tumor and normal voxels, four methods were used, containing MLP, linear SVM, nonlinear SVM, and Fuzzy. In this section, these methods briefly will be introduced. As mentioned above, there are two inputs for all these methods. These inputs contain a concentration of Cho and NAA.

As the first method, MLP has been chosen for classifying the voxels. This method is well suited to the classification of sets of input vectors into a set of corresponding output vectors. This neural network contains three layers: an input layer, hidden layer, and output layer . In this study, the input layer contains a concentration of Cho and NAA, and the hidden layer contains two or more neurons. The number of neurons depends on the context and the learning base. Finally, the output layer must show the best classification between normal and tumor voxels.
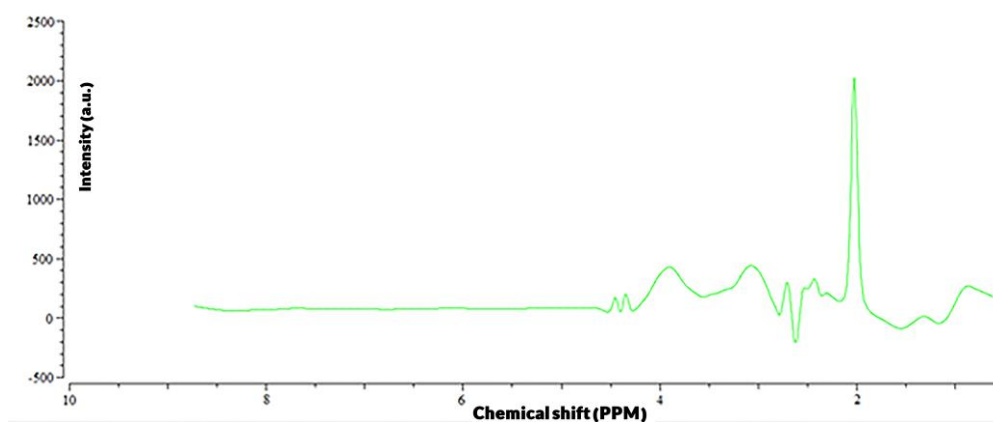

Figure 4. The representation of the NAA signal, which was used to determine where to fit the received signal
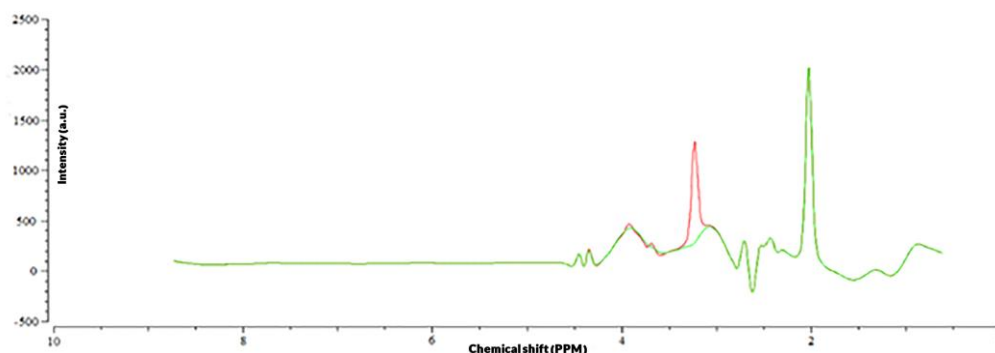

Figure 5. The red signal curve represents the model, and the green signal curve represents the phantom of the metabolite. Tarquin obtains each metabolite's concentration by calculating the area below the diagram of the regions associated with each metabolite

SVM is a supervised machine learning algorithm that can be used for both classification or regression challenges but it is mostly used for classification. In SVM problems, an n-dimension space will be used, where "n" is the number of input features and classification will be performed by finding the hyper-plane that makes the best differentiation between the two classes.

The fuzzy system typically contains a set of rules which demonstrates the relation between the input feature space and classes. In the fuzzy systems, the feature space is partitioned into multiple fuzzy subspaces by fuzzy if-then rules. These fuzzy rules can be represented by a network structure.

In this study fuzzy system is a multilayer feed-forward network consisting of the following layers: input, fuzzy membership, fuzzification, defuzzification, normalization, and output. The classifier has multiple inputs and multiple outputs.

3. Results

To extract the results, Tarquin was used for pre-processing and processing, while MATLAB was used for the final processing. Figure 6 shows the distribution of voxels. Red spots are healthy, and green spots are tumor patches.

The data in Figure 6 were used as input to neural networks, of which a certain number was used for training neural networks and some for testing neural networks.

Based on this selection, NAA and Cho were evaluated according to automatic diagnosis in the classification of voxels into two categories of tumors and healthy based on the function of SVM, MLP, Fuzzy with linear kernel, SVM with Gaussian kernel, and neural network (Table 1).
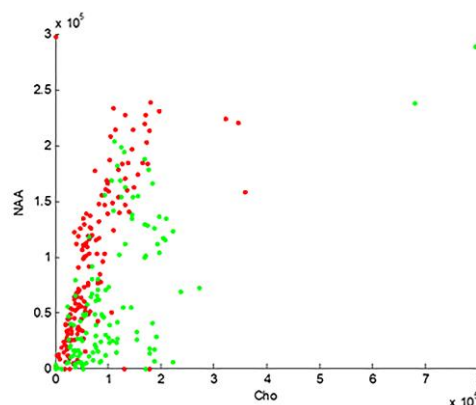

Figure 6. The distribution of healthy and tumor voxels. Red dots mark healthy voxels, while green dots mark tumor voxels

First, to determine the number of membership functions, the accuracy values of training and test data for neural networks with different numbers of membership functions were examined. Table 2 shows the accuracy values of training and test data.

4. Discussion

Tarquin was used in this study to remove the effects of water as well as macromolecules in MRS data. The reference spectra were then selected for fitting. MRS data with TE =135 ms included concentrations of several metabolites, the values of which can be measured with high accuracy after Tarquin analysis. In this study, corresponding with several studies' results, the concentrations of NAA and Cho metabolites, which have been used to differentiate between tumors and healthy vesicles, were used to train and test neural networks [27-30].

In this study, NAA and Cho metabolite concentrations were calculated and fed as input to neural networks. According to previous studies, the reason for using the concentrations of these metabolites was that they made a

Table 1. Accuracy, sensitivity, and specificity of neural networks studied

Classifier Type	Data Type	Accuracy	Sensitivity	Specificity
SVM with linear kernel	Train	65.6%	59.8%	72.9%
	Test	63%	56%	68%
Multi-Layer Perceptron	Train	81.1%	72.8%	87.7%
	Test	78.3%	66.7%	86.1%
Fuzzy system with 4 membership functions	Train	83.72%	82.9%	84.8%
	Test	82.5%	81.2%	84.5%
SVM with Gaussian Kernel	Train	89.7%	83.6%	94.6%
	Test	87%	82%	93%

Table 2. Training and test accuracy values with a number of different membership functions

Number of Membership functions	2	3	4	5	6
Training Accuracy	78.4%	80%	83.72%	89.6%	92%
Test Accuracy	76.74%	79.07%	82.5%	79.07%	74.42%

good distinction between healthy voxels and tumor voxels [27-30]. As the results showed, there is just a spatial estimation of tumor and normal tissue, so this discrimination would be used as a preprocessing step for more segmentation, which determines the boundaries between tumor and normal tissue. More segmentation would be used to fine segmenting the border of tissue.

As shown in Figure 1, the accuracy of the training increases with an increasing number of membership functions, and the accuracy of the test also increases with increasing the number of membership functions to 4, but with increasing to 5 and 6 membership functions, the accuracy of the test decreases. It can be claimed that when a fuzzy inference system becomes more complex, it becomes inaccurate, and no improvement in the overall accuracy of the system occurs. The accuracy of various training methods and testing methods was compared in reviewing and analyzing the experiment results.

As shown in Table 2, the accuracy of training increases with increasing membership functions, but the accuracy of testing for fuzzy neural networks with 5 and 6 membership functions decreases. According to these accuracy values, the best number of membership functions was equal to 4 functions.

A short glance at these results shows that accuracy obtained by using a support vector with the linear kernel is the lowest, while the highest accuracy is obtained using a support vector with Gaussian kernel, and from highest accuracy to lowest:

1. Backup vector with Gaussian kernel

2. Fuzzy logic

3. Multi-layer Perceptron

4. Backup vector with linear kernel

The analysis is as follows: considering the data type and its specifications, the support vector with Gaussian kernel shows the best and most appropriate complexity for data separation, and the fuzzy system and multi-layer perceptron also shows quality. However, since the fuzzy logic also uses Gaussian membership functions, it appears that the data used in this study would be better separated in Gaussian form. Therefore, it has higher accuracy than multi-layer Perceptron. Additionally, it is evident that the support vector's accuracy with the linear kernel is drastically reduced, which implies the data in this study is not linearly separable.

In the next step, the sensitivity and specificity data will be analyzed. The values are shown in Figure 7.

Figure 7 shows that in all cases, the sensitivity is lower than the specificity, which indicates the tumor patches are determined less accurately than healthy patches. On the other hand, it is understandable that the above data specifications are not optimal, and other metabolites are needed to separate the voxels. However, because of the data's complexity, it can be said that fewer specifications should be used in the data but with higher quality.
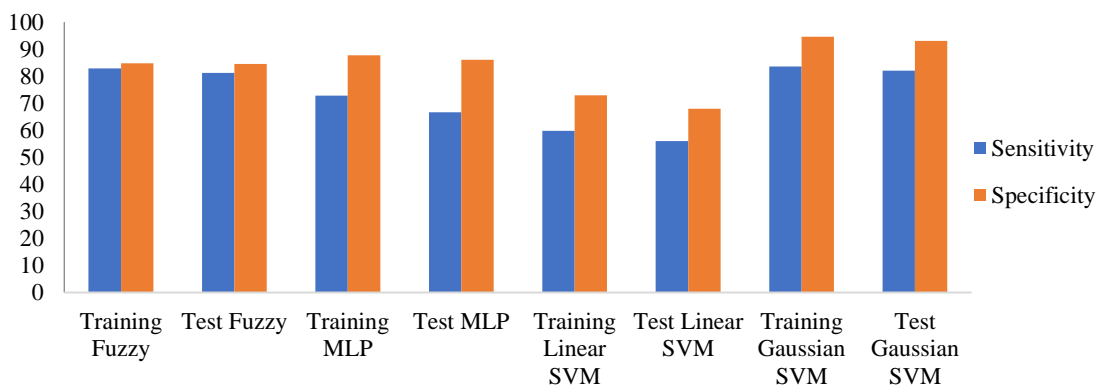

Figure 7. Comparison of sensitivity and specificity in different methods

References

1- L. L. Hintenlang *et al.*, "Treatment of a glioblastoma multiforme dural metastasis with stereotactic radiosurgery: A case report and select review of the literature," *Journal of Clinical Neuroscience*, vol. 48, pp. 118-121, 2018.

2- E. T. Ha *et al.*, "Chronic inflammation drives glioma growth: cellular and molecular factors responsible for an immunosuppressive microenvironment," vol. 1, pp. 66-76, 2014.

3- J. C. Peeken, J. Hesse, B. Haller, K. A. Kessel, F. Nüsslin, and S. E. J. S. u. O. Combs, "Semantic imaging features predict disease progression and survival in glioblastoma multiforme patients," vol. 194, no. 6, pp. 580-590, 2018.

4- P. Gandhi, R. Khare, H. VasudevGulwani, S. J. I. j. o. m. Kaur, and c. medicine, "Circulatory YKL-40 & NLR: Underestimated Prognostic Indicators in Diffuse Glioma," vol. 7, no. 2, p. 111, 2018.

5- H. Houson, B. Kasten, K. Jiang, J. Rao, and J. J. J. o. N. M. Warram, "MMP-14 as a noninvasive marker for PET and NIRF imaging of glioblastoma multiforme," vol. 60, no. supplement 1, pp. 1033-1033, 2019.

6- A. Allahverdi, S. Akbarzadeh, A. K. Moghaddam, and A. Allahverdy, "Differentiating Tumor and Edema in Brain Magnetic Resonance Images Using a Convolutional Neural Network," *Frontiers in Biomedical Technologies*, vol. 5, no. 1-2, pp. 44-50, 2018.

7- Y. Xia *et al.*, "Exploring the key genes and signaling transduction pathways related to the survival time of glioblastoma multiforme patients by a novel survival analysis model," *BMC genomics*, vol. 18, no. 1, p. 950, 2017.

8- T. N. Le *et al.*, "Characterization of an Orthotopic Rat Model of Glioblastoma Using Multiparametric Magnetic Resonance Imaging and Bioluminescence Imaging," *Tomography*, vol. 4, no. 2, p. 55, 2018.

9- E.-M. Ratai *et al.*, "ACRIN 6684: Multicenter, phase II assessment of tumor hypoxia in newly diagnosed glioblastoma using magnetic resonance spectroscopy," *PloS one*, vol. 13, no. 6, p. e0198548, 2018.

10- R. Wanner, A. Abaei, V. Rasche, and B. J. F. i. n. Knöll, "Three-dimensional in vivo Magnetic Resonance Imaging (MRI) of mouse facial nerve regeneration," vol. 10, 2019.

11- J. Klein, W. W. Lam, G. J. Czarnota, and G. J. J. O. Stanisz, "Chemical exchange saturation transfer MRI to assess cell death in breast cancer xenografts at 7T," vol. 9, no. 59, p. 31490, 2018.

12- W. T. Choi *et al.*, "Metabolomics of mammalian brain reveals regional differences," *BMC systems biology*, vol. 12, no. 8, p. 127, 2018.

13- G. Reynolds, M. Wilson, A. Peet, and T. N. J. M. R. i. M. A. O. J. o. t. I. S. f. M. R. i. M. Arvanitis, "An algorithm for the automated quantitation of metabolites in in vitro NMR signals," vol. 56, no. 6, pp. 1211-1219, 2006.

14- M. Wilson *et al.*, "Methodological consensus on clinical proton MRS of the brain: Review and recommendations," *Magnetic resonance in medicine*, vol. 82, no. 2, pp. 527-550, 2019.

15- A. G. Costigan, K. Umla-Runge, C. J. Evans, C. J. Hodgetts, A. D. Lawrence, and K. S. Graham, "Neurochemical correlates of scene processing in the precuneus/posterior cingulate cortex: A multimodal fMRI and 1H-MRS study," *Human brain mapping*, vol. 40, no. 10, pp. 2884-2898, 2019.

16- N. M. Simard, "TECHNICAL CONSIDERATIONS FOR 1H-MAGNETIC RESONANCE SPECTROSCOPY (1H-MRS) MEASUREMENT OF SPINAL CORD GAMMA-AMINOBUTYRIC ACID (GABA)," 2019.

17- S. Mitra *et al.*, "Proton magnetic resonance spectroscopy lactate/N-acetylaspartate within 2 weeks of birth accurately predicts 2-year motor, cognitive and language outcomes in neonatal encephalopathy after therapeutic hypothermia," *Archives of Disease in Childhood-Fetal and Neonatal Edition*, vol. 104, no. 4, pp. F424-F432, 2019.

18- D. Soares and M. Law, "Magnetic resonance spectroscopy of the brain: review of metabolites and clinical applications," *Clinical radiology*, vol. 64, no. 1, pp. 12-21, 2009.

19- A. Allahverdy, A. M. Nasrabadi, and M. R. Mohammadi, "Detecting ADHD children using symbolic dynamic of nonlinear features of EEG," *in Electrical Engineering (ICEE), 2011 19th Iranian Conference on*, 2011: IEEE, pp. 1-4.

20- M. F. Santarelli *et al.*, "How the signal-to-noise ratio influences hyperpolarized 13C dynamic MRS data fitting and parameter estimation," vol. 25, no. 7, pp. 925-934, 2012.

21- G. S. J. P. i. M. Payne and Biology, "Clinical applications of in vivo magnetic resonance spectroscopy in oncology," vol. 63, no. 21, p. 21TR02, 2018.

22- M. Wilson, G. Reynolds, R. A. Kauppinen, T. N. Arvanitis, and A. C. J. M. r. i. m. Peet, "A constrained least-squares approach to the automated quantitation of in vivo 1H magnetic resonance spectroscopy data," vol. 65, no. 1, pp. 1-12, 2011.

23- F. R. Lima-Junior and L. C. R. J. I. J. o. P. E. Carpinetti, "Predicting supply chain performance based on SCOR® metrics and multilayer perceptron neural networks," vol. 212, pp. 19-38, 2019.

24- S. Chen *et al.*, "Rapid determination of soil classes in soil profiles using vis–NIR spectroscopy and multiple objectives mixed support vector classification," vol. 70, no. 1, pp. 42-53, 2019.

25- A. A. Torres-García, C. A. Reyes-García, L. Villaseñor-Pineda, and G. J. E. S. w. A. García-Aguilar, "Implementing a fuzzy inference system in a multi-objective EEG channel selection model for imagined speech classification," vol. 59, pp. 1-12, 2016.

26- M. Jarrar, A. Kerkeni, A. B. Abdallah, and M. H. Bedoui, "MLP neural network classifier for medical image segmentation," *in 2016 13th International Conference on Computer Graphics, Imaging and Visualization (CGiV)*, 2016: IEEE, pp. 88-93.

27- S. Ulmer, M. Backens, and F. J. J. J. o. c. a. t. Ahlhelm, "Basic principles and clinical applications of magnetic resonance spectroscopy in neuroradiology," vol. 40, no. 1, pp. 1-13, 2016.

28- P. A. J. J. o. V. Keith and I. Radiology, "*ct and Mri of the Whole Body*, 2-volume Set," vol. 20, no. 10, p. 1397, 2009.

29- N. A. Parra *et al.*, "Volumetric spectroscopic imaging of glioblastoma multiforme radiation treatment volumes," vol. 90, no. 2, pp. 376-384, 2014.

30- H. Xu *et al.*, "Evaluation of neuron-glia integrity by in vivo proton magnetic resonance spectroscopy: Implications for psychiatric disorders," vol. 71, pp. 563-577, 2016.